

Sloshing induced impact with air cavity in rectangular tank with a high filling ratio

Olav F. Rognebakke and Odd M. Faltinsen
Centre for Ships and Ocean Structures
Norwegian University of Science and Technology
NO-7491 Trondheim, Norway

The motivation for the undergoing study is to better understand the sloshing induced impacts that may occur inside a container partially filled with liquid. Transport of liquefied natural gas (LNG) in prismatic membrane tanks exemplifies an area of application where impacting resonant waves cause loads that define the ultimate limit strength of the local structure. Model tests are usually performed with a small scale model, typically 1:50. Physical and economical considerations in general also restrict other test parameters, so that the liquid phase is water and the gas is air with a ullage pressure equal to the ambient atmospheric pressure. The model tank structure is made rigid, so that hydroelastic effects in the model tests are assumed to be negligible. Considering the differences in scale and physical parameters, the estimation of full-scale loads from model test pressure measurements is a great challenge. A detailed knowledge of the impact flow is a necessary premise.

High filling sloshing induced impacts are studied by experiments as well as by use of theoretical and numerical models. A two-dimensional flow is assumed in the theoretical treatment and aimed at in the experiments. The tank shape is rectangular. The idea in the experiments is to use high speed cameras and particle image velocimetry (PIV) technique to capture the details of the impact flow. Pressures are measured in the impact zone.

Categorization of impact types

The impact flow occurring for high filling sloshing with a right corner can be classified in three categories. For the highest filling ratios, even small excitation amplitudes for oscillatory motion with frequency content around the first linear eigenfrequency lead to impacts where a significant part of the tank roof is wetted. The free surface just prior to impact is characterized by a high curvature near the wall, which turns into a thin, fast jet shooting upwards and hitting the wall. The impact pressures are highly localized in the corner. This is denoted as the local vertical jet flow impact, Fig. 1. For lower filling ratios, or for an impact following a period with no impacts, the free surface may be smooth as the roof is hit. If the free surface curvature at the intersection with the tank wall is low, a flat impact occurs, Fig. 2. The resulting impact pressure is high. The narrow pressure peak moves rapidly out along the tank roof. This is the flat impact type. The final impact type is the impact with an air cavity in the corner between the tank wall and roof. This occurs when the free surface curves down towards the wall just before hitting the tank roof.

Impacts with air cavity

Figure 3 shows a schematic view of an impact with air cavity in the corner. This kind of impact occurs frequently for high filling ratio sloshing in rectangular tanks undergoing regular oscillatory translational motions. As a seemingly steady-state free surface motion is reached, the local free surface features in vicinity of the walls are complex. It appears that the previous tank roof impact in the same corner result in a flattening of the surface, which again leads

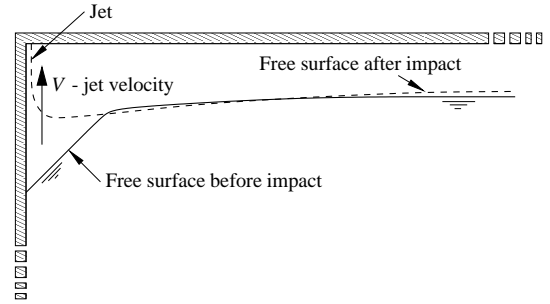


Figure 1: High curvature free surface impact with high velocity jet

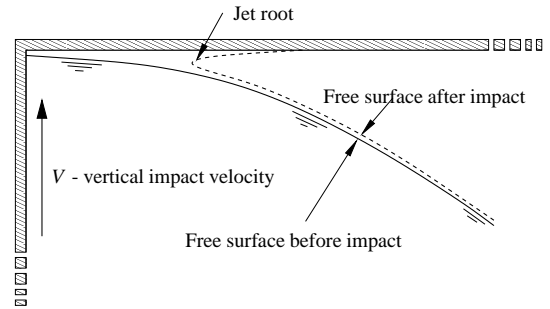


Figure 2: Flat impact

to a downward curving surface towards the wall and eventually the entrapment of an air cavity. An impact of this type is shown in Fig. 4. In this measurement, 1250 frames were captured per second, and the air cavity oscillation is clearly showing when the images are played back at a few frames per second.

Figure 5 shows the tank geometry and positioning of pressure sensors. The pressures are measured with a sampling frequency of 19.2kHz, and a filtering of 5kHz is applied. The trigger signal for the camera is also acquired, so that the pressures can be related to a given video frame. Measured pressures during the impact depicted in Fig. 4 are shown in Fig. 6. The air cavity oscillation is obvious, and the frequency is found from the power spectrum presented in to the right in Fig. 6. The frequency starts at about 90Hz, and is gradually increasing up to 120Hz as the size of the air cavity decreases. The change in size is probably due to a leakage of air through the pressure cell fittings. Calculation of the frequency of oscillation by use of a boundary element approach is presented in the following.

Numerical and theoretical treatment of entrapped air impact

Figure 7 shows an entrapped air pocket in the top right corner of a rectangular tank during sloshing induced impact. Figure 8 presents the boundary value problem, which is the basis for the bubble eigenvalue formulation. In the figure, the boundary condi-

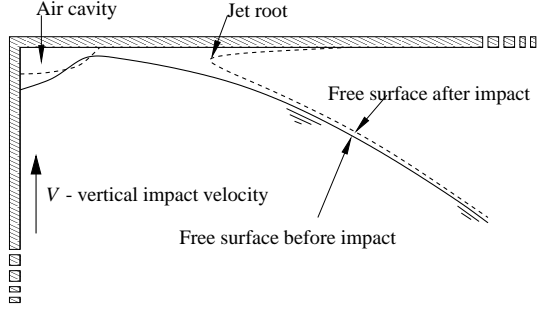


Figure 3: Impact with oscillating air cavity



Figure 4: Pictures of impact with air cavity

tions are satisfied on $z = 0$, which means that the wall condition $\partial\phi/\partial n = -\partial\phi/\partial z = 0$ where n is the unit normal vector pointing into the fluid. $\partial\phi/\partial n$ is used for generality. ϕ is the velocity potential in the fluid. C is a constant derived in the following. The vertical tank wall at the impact position is modeled by a mirroring about the z axis. The fluid acceleration is assumed to be much larger than the gravitational acceleration g , so that the linearized free surface condition is $\phi = 0$. The equation of continuity of the air cavity can be expressed as

$$\rho \frac{d\Omega}{dt} + \frac{d\rho}{dt} \Omega = 0. \quad (1)$$

Ω is the air cavity volume and ρ is the air density. The rate of change of the air pocket volume can be written as

$$\frac{d\Omega}{dt} = 2 \int_0^a \frac{\partial\phi}{\partial n} dx. \quad (2)$$

The factor 2 originates from the mirroring, as the air pocket volume in the calculations is two times the actual volume illustrated in Fig. 7. The encapsulated air is assumed to follow the adiabatic pressure-density relationship

$$\frac{p}{p_a} = \left(\frac{\rho}{\rho_a} \right)^\gamma, \quad (3)$$

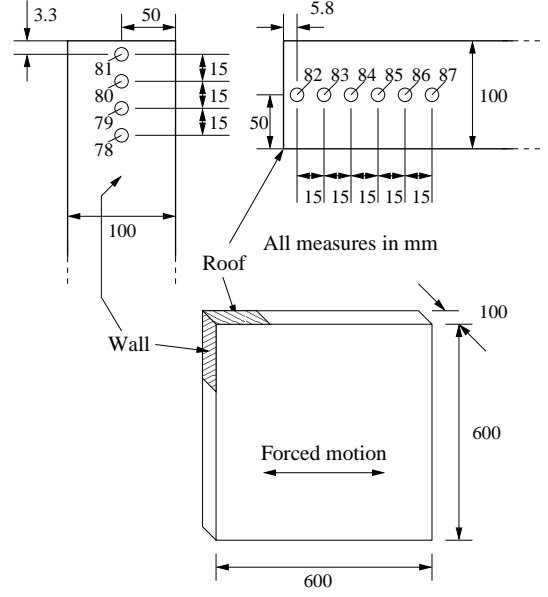


Figure 5: Position of pressure sensors in the tank

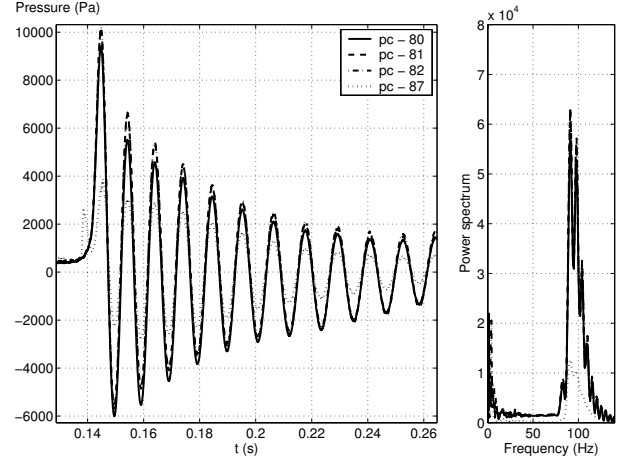


Figure 6: Measured pressures during impact with corresponding power spectrum

where p is air pocket pressure, which is assumed constant within the pocket volume. p_a and ρ_a are the pressure and density at the time of closure of the air pocket, respectively. A γ value of 1.4 is assumed. Equations (1) and (3) are linearized by expressing $p = p_a + p_1$ where $p_1/p_a \ll 1$. From a Taylor series expansion it follows that

$$\frac{\rho}{\rho_a} \simeq 1 + \frac{1}{\gamma} \frac{p_1}{p_a}. \quad (4)$$

The volume and density changes are small as a consequence of the previous assumption, which means that $(\Omega - \Omega_0)/\Omega \ll 1$ and $(\rho - \rho_a)/\rho \ll 1$. Ω_0 is the initial air pocket volume. The combined Eqs. (1), (2) and (3) give the change in air pressure

$$\frac{dp_1}{dt} = -2 \frac{\gamma p_a}{\Omega_0} \int_0^a \frac{\partial\phi}{\partial n} dx. \quad (5)$$

The free surface condition on the bubble is found from Bernoulli's equation. The fluid acceleration is assumed to be dominated by the compressibility effects of the air, so that the effect of gravity is neglected. The free surface condition is then linearized,

$$\rho_w \frac{\partial\phi}{\partial t} = p_a - p_w, \quad (6)$$

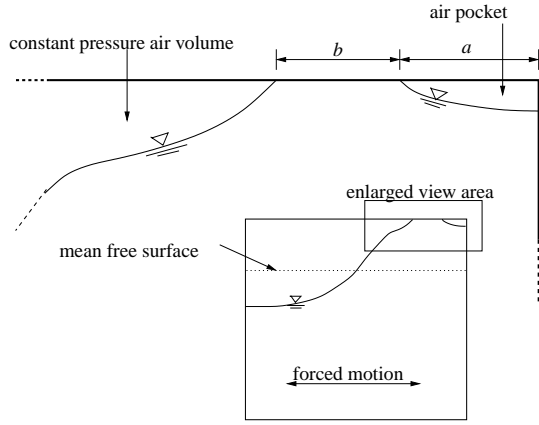


Figure 7: Entrapped air pocket during impact

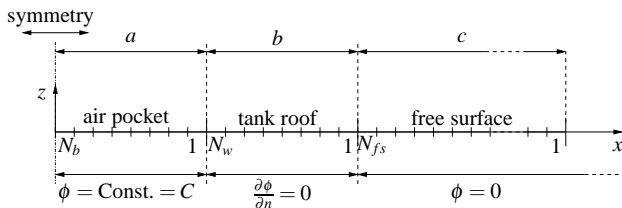


Figure 8: Boundary value problem and element discretization

where p_w and ρ_w are the pressure and density of the fluid, respectively. Surface tension is neglected. The pressure is continuous across the free surface, so that $p_w = p$. Using this and differentiating Eq. (6) with respect to time results in

$$\rho_w \frac{\partial^2 \phi}{\partial t^2} = -\frac{dp_1}{dt}. \quad (7)$$

Substitution of Eq. (5) results in

$$\frac{\partial^2 \phi}{\partial t^2} = 2 \frac{\gamma p_a}{\Omega_0 \rho_w} \int_0^a \frac{\partial \phi}{\partial n} dx. \quad (8)$$

The air pocket undergoes harmonic pressure, density and volume oscillations, so that $\partial^2 \phi / \partial t^2 = -\omega_n^2 \phi$, where ω_n is the natural frequency for the air pocket. The relation between ϕ and $\partial \phi / \partial n$ on the air pocket boundary is

$$\phi = -\frac{2}{\omega_n^2} \frac{\gamma p_a}{\Omega_0 \rho_w} \int_0^a \frac{\partial \phi}{\partial n} dx, \quad (9)$$

where ϕ is constant across the boundary.

Discretization and eigenvalue solution

Green's second identity is applied to the velocity potential. The velocity potential at a point $\mathbf{x} = (x, z)$ is

$$\phi(\mathbf{x}) = \frac{1}{2\pi} \oint_S \left(\phi(\boldsymbol{\xi}) \frac{\partial G(\mathbf{x}; \boldsymbol{\xi})}{\partial n} - G(\mathbf{x}; \boldsymbol{\xi}) \frac{\partial \phi(\boldsymbol{\xi})}{\partial n} \right) ds(\boldsymbol{\xi}), \quad (10)$$

where S is the boundary of the fluid domain. $s(\boldsymbol{\xi})$ is the integration variable along the boundary and $\boldsymbol{\xi} = (\xi, \zeta)$ is the (x, z) -coordinate of s along the boundary within the curve integral. G is the Rankine source.

The free surface, tank roof and air pocket surface are discretized using straight elements with constant source and normal velocity strength. This is illustrated in Fig. 8. $\partial \phi / \partial n$ is unknown on the

free surface and air pocket surface, while ϕ is unknown on the tank roof. The free surface is discretized over a length c , which is typically 10 times the size of the wetted wall section and the air pocket length combined ($a + b$). In the far-field, the effect of the oscillating air pocket is modeled by a vertical dipole in $x = 0$, so that the contribution from the free surface integral can be rewritten. The velocity potential for $x > a + b + c$ is approximated as

$$\phi \simeq \frac{Dz}{x^2 + z^2}. \quad (11)$$

D is a constant that is determined later. The integral for $a + b + c < x < \infty$ as well as the mirror contribution are evaluated by analytical expressions as described in (1). Assuming that the integration is along the horizontal axis so that $z = 0$, these contributions are

$$\begin{aligned} I_\infty &= D \int_{a+b+c}^{\infty} \frac{1}{x^2} G(\mathbf{x}; \boldsymbol{\xi}) dx \\ I_{-\infty} &= D \int_{-\infty}^{-(a+b+c)} \frac{1}{x^2} G(\mathbf{x}; \boldsymbol{\xi}) dx, \end{aligned} \quad (12)$$

where continuity in the vertical velocity across $x = a + b + c$ gives that the vertical dipole strength is

$$D = \frac{\partial \phi_j}{\partial z} \Big|_{j=N_{el}} (a + b + c)^2. \quad (13)$$

N_{el} is the total number of elements. The numerical approximation gives

$$\begin{aligned} 2\pi\phi(\mathbf{x}) &= \sum_{j=1}^{N_{el}} \left(\frac{\partial \phi}{\partial n} \right)_j \int_{\delta s_j + \delta \bar{s}_j} G(\mathbf{x}; \boldsymbol{\xi}) ds \\ &\quad - \sum_{j=1}^{N_{el}} \phi_j \int_{\delta s_j + \delta \bar{s}_j} \frac{\partial G(\mathbf{x}; \boldsymbol{\xi})}{\partial n} ds \\ &\quad - (I_{-\infty} + I_\infty), \end{aligned} \quad (14)$$

where ϕ_j and $(\partial \phi / \partial n)_j$ are the constant velocity potential and normal velocity for element j , respectively. $\delta \bar{s}_j$ is the mirror element about the z axis from δs_j . Equation (14) is set up for $\mathbf{x} = \mathbf{x}_i$ at the center of each element, which gives

$$2\pi\phi(\mathbf{x}_i) = \sum_{j=1}^{N_{el}} \left(\frac{\partial \phi}{\partial n} \right)_j B_{ij} - \sum_{j=1}^{N_{el}} \phi_j A_{ij}, \quad (15)$$

where

$$A_{ij} = \int_{\delta s_j + \delta \bar{s}_j} \frac{\partial G(\mathbf{x}_i; \boldsymbol{\xi})}{\partial n} ds, \quad i, j = 1 \dots N_{el}, \quad (16)$$

$$\begin{aligned} B_{i=1 \dots N_{el}, j=1} &= \\ &\int_{\delta s_j + \delta \bar{s}_j} G(\mathbf{x}_i; \boldsymbol{\xi}) ds - (a + b + c)^2 (I_{-\infty} + I_\infty), \end{aligned} \quad (17)$$

$$B_{i=1 \dots N_{el}, j=2 \dots N_{el}} = \int_{\delta s_j + \delta \bar{s}_j} G(\mathbf{x}_i; \boldsymbol{\xi}) ds, \quad (18)$$

The boundary conditions are used to set up the eigenvalue problem.

$$\begin{aligned} \kappa_i 2\pi\phi_i - \sum_{j \in (FS, B)} \left(\frac{\partial \phi}{\partial n} \right)_j B_{ij} + \sum_{j \in W} \phi_j A_{ij} &= \\ -\lambda \sum_{i \in B} \left(\frac{\partial \phi}{\partial n} \right)_j K_{ij}, \end{aligned} \quad (19)$$

where FS is the set of all free surface elements, W is the set of all elements on the tank roof, B is the set containing air pocket elements and

$$\kappa_i = \begin{cases} 0 & i \in (FS, B) \\ 1 & i \in W \end{cases}. \quad (20)$$

The coefficients K_{ij} and λ are derived in the following manner. The sum over the air pocket elements with contribution from the velocity potential is the starting point.

$$\sum_{j \in B} \phi_j A_{ij} = \phi_b \sum_{j \in B} A_{ij} = \phi_b F_i, \quad (21)$$

where ϕ_b is the constant velocity potential on the air pocket boundary. Inserting for ϕ_b from Eq. (9) results in

$$\sum_{j \in B} \phi_j A_{ij} = \frac{1}{\omega_n^2} \frac{2\gamma p_a}{\rho_w \Omega_0} F_i \int_{S_B} \frac{\partial \phi}{\partial n} ds. \quad (22)$$

S_B is the air pocket boundary. A reasonable approximation of the integration of the normal velocity on S_B can be performed by a simple summation,

$$\int_{S_B} \frac{\partial \phi}{\partial n} ds = \sum_{j \in B} \left(\frac{\partial \phi}{\partial n} \right)_j \Delta s_j, \quad (23)$$

Δs_j is the length of element j . The combination of Eqs. (21), (22) and (23) compared to Eq. (19) leads to the following expressions,

$$K_{ij} = \frac{2\gamma p_a}{\rho_w \Omega_0} F_i \Delta s_j, \quad (24)$$

and

$$\lambda = \frac{1}{\omega_n^2}. \quad (25)$$

The system of equations in Eq. (19) is put in matrix form

$$M \mathbf{y} = \lambda N \mathbf{y}, \quad (26)$$

and a standard mathematical library utilizing the QZ algorithm is used to determine the eigenvalues λ and the corresponding eigenvectors.

The free surface velocity has a square root singularity at the intersection points between the free surface and tank wall and tank wall and air pocket, as long as the intersection line is horizontal. In order to increase the accuracy of the numerical solution, the element size is made smaller towards the singularities.

Results

Two types of element discretizations are used; one with all elements on $z = 0$ and one where the air cavity elements are situated on the arc of an ellipsoid extending down to $z = -a/4$. Figure 9 presents the eigenmodes for an air pocket with the same length as the wetted part of the tank roof, $a = b = 0.05\text{m}$, as well as the air pocket frequency as a function of the air pocket length divided by the wetted tank roof length, a/b . The wetted tank roof length is $b = 0.05\text{m}$ in the calculations. A total of 180 panels are used. An analytical expression for the air cavity resonance frequency is developed by Faltinsen (2) for a related problem, where an air pocket is entrapped below a structure during a wave impact. The basis for the analytical result is a slightly different boundary value problem, where the boundary with a zero normal velocity has a given length at one side of the air cavity but goes to infinity at the other side. A constant normal velocity across the air cavity is also assumed. The analytical result for the frequency is between the two curves based on a numerical solution. The eigenmodes, which represent the oscillation mode, are similar for the air cavity modeled by elements on $z = 0$ and elements positioned on an elliptical cavity. The difference is in the change of sign of $\partial \phi / \partial n$ for the elliptical cavity close to the roof intersection singularity. Table 1 presents the eigenfrequency of the air cavity for different calculation methods. It is now interesting to compare these results with the experimental findings of Fig. 5-6. The real air cavity has

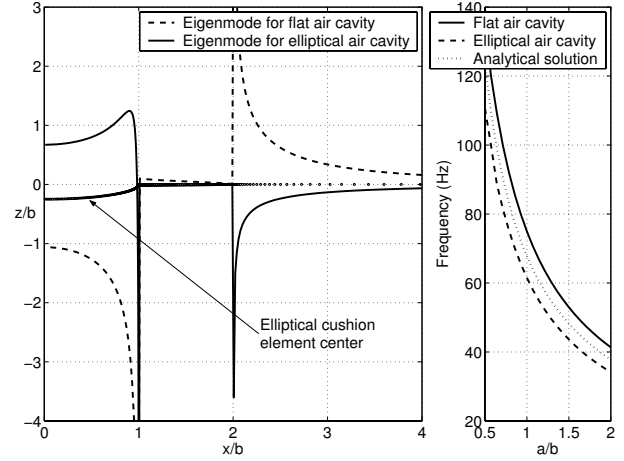


Figure 9: The left figure shows eigenmodes for $a = b = 0.05\text{m}$. To the right is the air cavity frequency as a function of a/b for $b = 0.05\text{m}$. Flat cavity calculations with $N_{fs} = 80$, $N_w = 50$ and $N_b = 50$, while elliptical cavity calculations are with $N_{fs} = 50$, $N_w = 50$ and $N_b = 80$

Table 1: Calculated air cavity frequency

Air cavity geometry		Elements on $z = 0$	Elements on ellipsoid arc	Analytical result
a (m)	b (m)	(Hz)	(Hz)	(Hz)
0.025	0.05	82.9	68.4	75.5
0.05	0.05	75.0	61.5	67.8
0.05	0.025	136.3	110.7	123.5
0.025	0.025	150.1	123.3	135.6

three-dimensional features, but let us assume an average length of 0.05m in the excitation direction. The wetted part of the tank roof has a comparable length as the extent of the cavity for a significant number of oscillations. The calculated air cavity frequency from the eigenvalue problem with elements at $z = 0$ and $b = a = 0.05\text{m}$ is 75Hz . This is a reasonable estimate of the measured frequency of around 90Hz .

Concluding remarks

The eigenvalue solution based on a boundary element approach can be used to predict the eigenfrequency of an air cavity entrapped during a sloshing induced impact. In order to determine the pressure magnitude, a nonlinear BEM can be applied. This involves solving for the full sloshing flow up to and beyond the time of impact.

Acknowledgements

This work is performed by Centre for Ships and Ocean Structures, and the authors are grateful for the funding of this centre provided by the Research Council of Norway.

References

- [1] FALTINSEN, O. M. (1977) Numerical solutions of transient nonlinear free-surface motion outside or inside moving bodies. *Proc. 2nd Intern. Conf. of Numerical Ship Hydrodynamics*, Univ. of California, Berkeley, University Extension Publisher, pp 347–357.
- [2] FALTINSEN, O. M. (2005) *Hydrodynamics of High-Speed Marine Vehicles*. New York: Cambridge University Press.